

See discussions, stats, and author profiles for this publication at: <https://www.researchgate.net/publication/224017341>

# Deactivating Species Deposited on Pt–Pd Catalysts in the Hydrocracking of Light–Cycle Oil

ARTICLE in ENERGY & FUELS · FEBRUARY 2012

Impact Factor: 2.79 · DOI: 10.1021/ef2019676

CITATIONS

20

READS

16

6 AUTHORS, INCLUDING:



Pedro Castaño

Universidad del País Vasco / Euskal Herriko U...

71 PUBLICATIONS 838 CITATIONS

SEE PROFILE



A. Gutierrez

Universidad del País Vasco / Euskal Herriko U...

21 PUBLICATIONS 136 CITATIONS

SEE PROFILE



Idoia Hita

Universidad del País Vasco / Euskal Herriko U...

8 PUBLICATIONS 42 CITATIONS

SEE PROFILE



Andrés T. Aguayo

Universidad del País Vasco / Euskal Herriko U...

155 PUBLICATIONS 3,840 CITATIONS

SEE PROFILE

# Deactivating Species Deposited on Pt–Pd Catalysts in the Hydrocracking of Light-Cycle Oil

Pedro Castaño,\* Alazne Gutiérrez, Idoia Hita, José M. Arandes, Andrés T. Aguayo, and Javier Bilbao

Department of Chemical Engineering, University of the Basque Country (UPV/EHU), Post Office Box 644, 48080 Bilbao, Spain

**ABSTRACT:** The nature and composition of the coke deposited on Pt–Pd catalysts supported on acid carriers during the hydroprocessing (hydrocracking and hydrotreating) of light-cycle oil (LCO) has been studied. Five types of supports have been used: a commercial cracking catalyst, alumina, H $\beta$  zeolite, and two HY zeolites (with different acidities). The hydrocracking runs have been performed at 350 °C and 50 bar for up to 24 h. The characterization of the deactivating species on the catalyst used has been performed using temperature-programmed oxidation (TPO) coupled with mass spectrometry (MS) and Fourier transformed infrared (FTIR) spectroscopy, ultraviolet–visible (UV–vis) spectroscopy, and comprehensive two-dimensional gas chromatography/mass spectrometry (GC  $\times$  GC/MS) analysis of the soluble coke extracted from the deactivated catalyst. The complex composition of the coke has been simplified in three families, each related to a different composition and location. The composition of the coke (and the amount of each type of coke) strongly depends upon the catalyst properties, particularly the features of the support: acidity and micropore topology.

## 1. INTRODUCTION

Hydrocracking is considered a key process in the refineries for increasing the yield of middle distillates, reducing at the same time the amount of aromatics and sulfur.<sup>1</sup> These features are particularly interesting when heavy crudes, bitumens, shales, and wastes are the raw materials for the biorefining industry. Because of its versatility, hydrocracking is suitable for producing middle distillates from secondary refinery streams [residues, atmospheric distillation gas oil, light-cycle oil (LCO) from fluid catalytic cracking (FCC) units, and others].<sup>2,3</sup> It is also suitable for treating renewable feeds, such as vegetable oils,<sup>4,5</sup> and waxes from Fischer–Tropsch synthesis.<sup>6</sup> Accordingly, intensive research is being undertaken on novel catalytic designs,<sup>7–14</sup> as well as the mechanistic and kinetic modeling of hydrocracking.<sup>15–17</sup>

The hydrocracking of LCO (byproduct of the FCC) concentrates great interest. The FCC unit is continuously subjected to revamping for increasing the production and quality of its products (gasoline and light olefins) and adapting to the co-feeding of new streams (such as biomass derivatives) and streams from hydroprocessing units.<sup>18</sup> Besides, the LCO cannot be directly added to the diesel pool because of its high aromatic and sulfur content and its low stability.<sup>19</sup> In the literature, the hydrocracking of LCO has been studied using model compounds,<sup>20</sup> light fractions of LCO,<sup>21</sup> LCO diluted with other refinery streams,<sup>22</sup> and pre-hydrotreated LCO.<sup>23–25</sup> Recent works on the hydrocracking of straight LCO have revealed that the activity of noble metal catalysts (Pt, Pd, and Pt–Pd) is related to the support acidity, achieving high conversion values with H $\beta$  and HY zeolites as supports.<sup>26</sup>

Catalyst deactivation is one of the main obstacles for industrial implementation of the hydrocracking of the LCO process using noble-metal-supported catalysts. It has been shown that deactivation occurs in the initial 5 h on stream, and then a pseudo-stable activity regime is reached. This state corresponds to a zero deactivation rate because of the auto-

regeneration capacity of the catalyst with hydrogen. The remaining activity of the catalyst in the pseudo-stable state depends upon the reaction conditions and catalyst properties.<sup>26–29</sup>

The causes of deactivation are coke fouling and poisoning (by sulfur and nitrogen). The Pt–Pd bimetallic catalysts are more suitable for enhancing resistance toward sulfur poisoning than the monometallic counterparts. Furthermore, coke deposition is affected by different properties of the support: (i) porous structure, (ii) total acidity, and (iii) acid strength of the acid sites. The catalysts based on H $\beta$  and HY zeolites are very active for hydrocracking and also for coke formation because of their capacity of condensing reactants and hydrocracking products. Besides, these catalysts based on acid zeolites are also more active in the hydrocracking of coke precursors, and therefore, their remaining activity in the pseudo-stable state is higher than that of the catalysts based on less acid supports.<sup>26,27</sup>

This study addresses the composition and properties of the deactivating species deposited on noble-metal-supported catalysts. The term “deactivating species” includes coke and molecules with sulfur and nitrogen adsorbed/retained on the catalysts. The deactivation during the cracking processes will be monitored<sup>30,31</sup> and discussed in terms of differences in catalytic properties, complex composition of the feed or reaction conditions. The results are of interest toward a rational design of bifunctional catalysts and kinetic modeling.

## 2. EXPERIMENTAL SECTION

**2.1. LCO Properties.** The LCO has been provided by Repsol YPF and analyzed by different methods: (i) elemental analysis in a EuroVector Euro EA elemental analyzer (CHNS), (ii) X-ray fluorescence (XRF) in a Philips MiniPal PW-4025, (iii) American

Received: December 16, 2011

Revised: January 19, 2012

Published: January 21, 2012



Society for Testing and Materials (ASTM) D4052 for measuring the density, (iv) ASTM D4737 for measuring the cetane index, (v) ASTM D2887 for obtaining the simulated distillation curve, and (vi) chromatography for the composition in an Agilent 7890A GC ×

**Table 1. Properties of the LCO**

density (kg L <sup>-1</sup> ) (ASTM D4052)	0.936
simulated distillation (ASTM D2887)	
IBP–FBP (°C)	101.5–466.0
T <sub>10</sub> (°C)	210
T <sub>30</sub> (°C)	240
T <sub>50</sub> (°C)	277
T <sub>70</sub> (°C)	322
T <sub>90</sub> (°C)	374
cetane number (ASTM D4737)	27.64
chemical analysis (wt %)	
C	88.8
H	10.4
S	0.6
N	0.2
composition (wt %)	
isoparaffins	5.18
paraffins	5.43
olefins	1.55
naphthenes	0.39
dinaphthenes	0.42
aromatics	66.83
polyaromatics	5.12
acenahthenes	0.19
fluorenes	2.08
indanes + indenenes	5.53
others	7.28

GC. The properties of the LCO are summarized in Table 1. As displayed, the concentrations of nitrogen and sulfur are 0.2 and 0.6 wt %, respectively, whereas the boiling point of the feed (distillation curve) is suitable for attaining a trickle-bed regime within the standard hydroprocessing conditions.

Comprehensive two-dimensional gas chromatography (GC × GC) coupled with mass spectrometry (MS) has been used for analyzing the feed, the products, and the soluble coke. The equipment used (Agilent 7890A and Agilent 5975C series GC/MSD) consists of two columns of different polarities connected through a flow modulator. The first column is a nonpolar DB-5 ms J&W 122-5532 (length, 30 m; internal diameter, 0.25 mm), whereas the second column is a polar TRB-50 HT (length, 6 m; internal diameter, 0.25 mm). The outlet flow of the sample and carrier is connected to a flame ionization detector (FID) and a mass selective detector (MSD); the identification of the components has been carried out using the National Institute of Standards and Technology (NIST) 05 library. The chromatographic methods have been described in Table 2. Figure 1 shows the composition of the LCO determined from GC × GC/FID results. Given that 99.2 wt % of the LCO is C and H, the contour map displayed in Figure 1 is associated with the fraction in weight of each component. The segregation on the *x* axis (corresponding to the first column) is attributed to the retention time and, therefore, linked with the boiling point of the components. The segregation on the *y* axis (second-column separation) is attributed to the different polarity and, therefore, linked with the number of insaturations or the presence of heteroatoms in the molecule. The resulting chromatogram shows that the LCO is composed of 70 wt % aromatics. The most abundant family is diaromatics (substituted naphthalene and biphenyl) with values of ca. 30 wt %, but there are also tri- and monoaromatics with long aliphatic chains. Among the monoaromatics, the most abundant compounds are 1,1-dimethyl-2-propenyl benzene and 1-methyl-3-(1-

**Table 2. Parameters of the Chromatographic Method by GC × GC/MS**

parameter	
injector temperature (°C)	350
volume of the sample injected (μL)	10
split	5:1
flow toward MSD (mL min <sup>-1</sup> )	0.75
flow toward FID (mL min <sup>-1</sup> )	21 <sup>a</sup> or 25 <sup>b</sup>
modulation period (s)	1.48
FID temperature (°C)	350
interphase temperature (°C)	300
ion source temperature (°C)	300
oven initial temperature (°C)	50
time at initial temperature (min)	5
oven ramp (°C min <sup>-1</sup> )	3
oven final temperature (°C)	310
time at final temperature (min)	30

<sup>a</sup>Flow used in the analysis of the LCO and hydrocracking products.

<sup>b</sup>Flow used in the analysis of soluble coke.

methyl-2-propenyl) benzene. The most abundant compounds among the triaromatics are substituted anthracenes and phenantrenes. The presence of aromatics of more than four rings is not as significant as that of the remaining aromatics; i.e., only few compounds, mainly pyrenes, have been detected.

**2.2. Catalyst Preparation and Properties.** Five bifunctional catalysts have been prepared from different supports with different acidity and shape selectivity: Y<sub>12</sub> (HY ultrastable zeolite, CBV712, Zeolyst International, SiO<sub>2</sub>/Al<sub>2</sub>O<sub>3</sub> = 12), Y<sub>5</sub> (HY ultrastable zeolite, CBV500, Zeolyst International, SiO<sub>2</sub>/Al<sub>2</sub>O<sub>3</sub> = 5), B (Hβ zeolite, CP814E, SiO<sub>2</sub>/Al<sub>2</sub>O<sub>3</sub> = 25), F (a commercial equilibrated FCC catalyst, Albemarle), and A (amorphous γ-alumina, Stem Chemicals). The acid supports were supplied in ammonium form, and therefore, to obtain their acid form, they have been calcined according to the following steps: (i) 2 h at 400 °C (5 °C min<sup>-1</sup>), (ii) 15 h at 500 °C (5 °C min<sup>-1</sup>), and (iii) 2 h at 550 °C (5 °C min<sup>-1</sup>).

The supports have been impregnated at 80 °C with an aqueous solution of Pt(NH<sub>3</sub>)<sub>4</sub>(NO<sub>3</sub>)<sub>2</sub> (Alfa Aesar) and Pd(NH<sub>3</sub>)<sub>4</sub>(NO<sub>3</sub>)<sub>2</sub> (Stem Chemicals). The amount of noble metal solution required is added to 100 mL of deionized water by keeping pH at 7. Once adsorption equilibrium has been reached, the excess of water is removed in a rotavapor. The catalyst obtained is dried in an oven for 24 h at 120 °C and, subsequently, calcined with air at 450 °C (following a ramp of 5 °C min<sup>-1</sup>) for 2 h.

The properties of the fresh catalysts are shown in Table 3. The metal content of the bifunctional catalysts has been determined by inductively coupled plasma–atomic emission spectroscopy (ICP–AES) in a HORIBA Jobin Yvon. The samples have previously been subjected to acid digestion with HF (Merck) at 90 °C. The volume of pores [*V<sub>p</sub>*, using the Barrett–Joyner–Halenda (BJH) method], the volume of micropores (*V<sub>mp</sub>*), and the surface area [*S<sub>g</sub>*, using the Brunauer–Emmett–Teller (BET) method] have been determined by N<sub>2</sub> adsorption–desorption isotherms. The analyses have been performed at –196 °C in a Micromeritics ASAP 2010 once the samples have been degassed under a vacuum at 150 °C for 8 h. The metal surface area (*S<sub>m</sub>*) and the metallic particle size (*d<sub>m</sub>*) have been determined by H<sub>2</sub> chemisorption at 100 °C<sup>32</sup> according to the double isotherm method<sup>33</sup> in a Micromeritics AutoChem II. The acidity (*α*) and average acid strength (*S<sub>a</sub>*) have been measured by temperature-programmed desorption (TPD) of NH<sub>3</sub> adsorbed at 150 °C in a TG-DSC Setaram 111 calorimeter, provided with a Harvard syringe, and an online Balzers Quadstar 422 mass spectrometer. Prior to analysis, each sample is subjected to sweeping with He at 550 °C for 0.5 h for impurity removal. It is then cooled to 150 °C, and a NH<sub>3</sub> flow of 50 μL min<sup>-1</sup> is introduced. Once the sample has been saturated, NH<sub>3</sub>–TPD is carried out and desorption is quantified by means of a Balzers Quadstar 422 spectrometer. Accordingly, a He flow of 20 mL min<sup>-1</sup> is

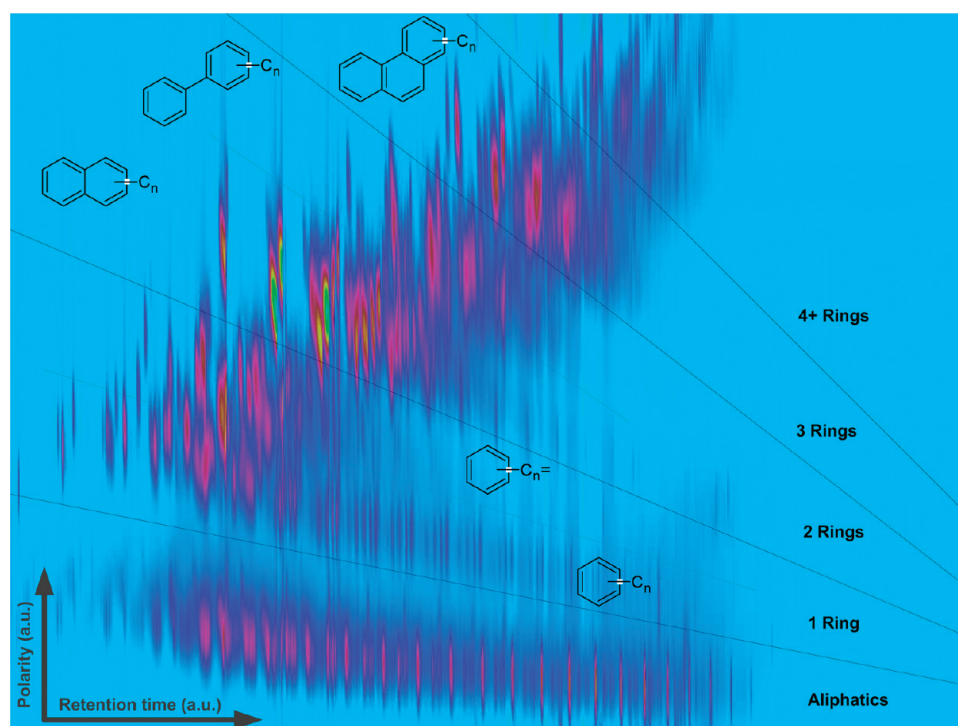


Figure 1. Results of the LCO analysis by GC  $\times$  GC using the FID.

Table 3. Properties of the Fresh Catalysts

catalyst	F	A	B	Y <sub>12</sub>	Y <sub>5</sub>
support	FCC catalyst	$\gamma$ -Al <sub>2</sub> O <sub>3</sub>	H $\beta$ zeolite	HY zeolite	HY zeolite
SiO <sub>2</sub> /Al <sub>2</sub> O <sub>3</sub>	4		25	12	5.2
Pt (wt %)	0.45	0.46	0.67	0.63	1.12
Pd (wt %)	0.42	0.37	0.57	0.58	0.46
V <sub>p</sub> (cm <sup>3</sup> g <sub>cat</sub> <sup>-1</sup> )	0.14	0.48	0.80	0.34	0.40
V <sub>mp</sub> (cm <sup>3</sup> g <sub>cat</sub> <sup>-1</sup> )	0.02	0.06	0.15	0.18	0.25
S <sub>g</sub> (m <sup>2</sup> g <sub>cat</sub> <sup>-1</sup> )	90	285	562	511	668
S <sub>m</sub> (m <sup>2</sup> g <sub>cat</sub> <sup>-1</sup> )	0.33	0.37	0.09	0.26	0.85
d <sub>m</sub> (nm)	8	6	6	5	5
$\alpha$ ( $\mu$ mol <sub>NH<sub>3</sub></sub> g <sub>cat</sub> <sup>-1</sup> )	65	347	598	550	686
$\alpha_{\text{weak}}$ ( $\mu$ mol <sub>NH<sub>3</sub></sub> g <sub>cat</sub> <sup>-1</sup> )	35	100	84	90	311
$\alpha_{\text{medium}}$ ( $\mu$ mol <sub>NH<sub>3</sub></sub> g <sub>cat</sub> <sup>-1</sup> )	27	195	448	385	252
$\alpha_{\text{strong}}$ ( $\mu$ mol <sub>NH<sub>3</sub></sub> g <sub>cat</sub> <sup>-1</sup> )	3	52	66	75	123
S <sub>a</sub> (kJ mol <sub>NH<sub>3</sub></sub> <sup>-1</sup> )	65	80	87	98	109
B/L	0.40	0.48	0.49	0.70	0.68

passed at the same time as the temperature is raised to 550 °C, following a heating ramp of 5 °C min<sup>-1</sup>.<sup>34</sup> Different acidity levels have been established according to their intrinsic desorption temperature:<sup>35,36</sup> (i) weak, 150–280 °C; (ii) medium, 280–420 °C; and (iii) strong, 420–550 °C. The ratio of Brønsted/Lewis (B/L) sites has been determined by means of Fourier transform infrared (FTIR) spectroscopic analysis of adsorbed pyridine. The analysis has been carried out in a Nicolet 740 SX FTIR provided with a Specac transmission catalytic cell equipped with a temperature controller and a vacuum pump. The ratio has been calculated from the vibrational bands of pyridine adsorbed at 1547 cm<sup>-1</sup> (pyridine associated with Brønsted sites) and 1455 cm<sup>-1</sup> (pyridine associated with Lewis sites) using their molar extinction coefficients.<sup>37</sup> Prior to the analysis, a pellet made up of approximately 1 mg of sample and KBr is subjected to

vacuum at 400 °C for 0.5 h. The sample is then saturated with pyridine at 150 °C, and the spectrum is recorded.

The Pt content of the bifunctional catalysts varies between 0.45 and 1.12 wt %, whereas the Pd content varies between 0.37 and 0.58 wt %. The highest value of the pore volume (V<sub>p</sub>) is for the B catalyst (Pt–Pd/H $\beta$ ) with almost a double value than the others. On the other hand, the F catalyst has values as low as 0.14 cm<sup>3</sup> g<sub>cat</sub><sup>-1</sup>. The Y catalysts (both Y<sub>5</sub> and Y<sub>12</sub>) show the highest values of micropore volume (V<sub>mp</sub>), 0.18–0.25 cm<sup>3</sup> g<sub>cat</sub><sup>-1</sup>, which means that more than 60% of the pore volume corresponds to micropores. This percentage drops to 18, 14, and 12.5% for B, F, and A catalysts, respectively. The surface area (S<sub>g</sub>) and micropore volume (V<sub>mp</sub>) have the same trend. The accessible metallic surface is very high (0.85 m<sup>2</sup> g<sub>cat</sub><sup>-1</sup>) for the Y<sub>5</sub> catalyst, whereas it is very low for the B catalyst (0.09 m<sup>2</sup> g<sub>cat</sub><sup>-1</sup>), approximately 10% of the accessible metallic function of the former. The values of acidity, acid strength, and B/L site ratio lead to the conclusion that Y catalysts are the most acidic catalysts (with values 10 times greater than those for the F catalyst), whereas B and A catalysts have a higher fraction of medium acidity.

**2.3. Hydrocracking Unit and the Analysis of Products.** The reaction equipment used has been described elsewhere.<sup>26,38,39</sup> It is equipped with a down-flow fixed-bed reactor of 15 cm<sup>3</sup> (8 mm internal diameter and 303 mm length). The reaction conditions are 350 °C, 50 bar, H<sub>2</sub>/LCO molar ratio ( $n_{\text{H}_2}$ ) of 8.9 mol<sub>H<sub>2</sub></sub> mol<sub>LCO</sub><sup>-1</sup>, weight hourly space velocity (WHSV) of 4 h<sup>-1</sup>, and time on stream (TOS) of 300 min. Prior to the reaction, the catalyst (0.15–0.30 mm pellets), mixed (1:1 mass ratio) with CSI (0.5 mm), is activated *in situ* under atmospheric pressure with a stream of the H<sub>2</sub>/N<sub>2</sub> mixture (30 mL min<sup>-1</sup> of H<sub>2</sub> and 50 mL min<sup>-1</sup> of N<sub>2</sub>), raising the temperature following a ramp of 5 °C min<sup>-1</sup> from ambient temperature to 350 °C and keeping this temperature for 4 h. To avoid gas bypassing and heat losses, CSI layers of around 20 mm thickness are placed above and below the catalyst bed.

The reaction products are sent to a gas/liquid separator, and the gases are analyzed online in a Varian CP-4900 microGC provided with four channels: (i) a molecular sieve to separate the permanent gases H<sub>2</sub>, O<sub>2</sub>, N<sub>2</sub>, methane, and CO<sub>2</sub>, (ii) a Porapak Q to separate C<sub>2</sub> hydrocarbons, CO<sub>2</sub>, and H<sub>2</sub>S, (iii) Al<sub>2</sub>O<sub>3</sub> to separate C<sub>3</sub> and C<sub>4</sub> hydrocarbons, and (iv) CPSiL to separate C<sub>5</sub>–C<sub>10</sub> hydrocarbons. The



liquids are analyzed in a Hewlett-Packard 6890 gas chromatograph provided with a FID and a PONA capillary column (50 m  $\times$  2 mm  $\times$  0.5 mm).

**2.4. Coke Characterization.** To obtain information regarding the properties of the coke, we have combined the temperature-programmed oxidation (TPO) with thermogravimetry (TG), MS, and FTIR spectroscopy. TG analysis has been performed in a thermobalance (TA Instruments SDT 2960), MS has been performed in a quadrupole (Balzers Instruments Thermostar) attached to the previous thermobalance. FTIR measurements have been carried out in a Nicolet 6700 (Thermo) with a sample transmission cell (Specac). All TPO curves have been obtained using 10–20 mg of crushed deactivated catalyst, with an initial stripping of impurities under a continuous flow of He and 550 °C, and using a ramp of 3 °C min<sup>-1</sup>. In the case of FTIR, the samples have been mixed with KBr, pelletized, and then pretreated under vacuum.

Ultraviolet–visible (UV–vis) spectroscopy spectra have been obtained in a Varian Cary 5000, equipped with an integration cell, in the 200–900 nm range. The sample (1–3 mg) has been crushed prior to analysis.

The soluble coke has been extracted from the deactivated catalyst following a procedure optimized by modifying a procedure in the literature:<sup>40,41</sup> (i) 0.3–0.5 g of sample of spent catalyst has been exposed to 5 mL of HF (Merck, 40%) to destroy the structure of the zeolite; (ii) the sample has been neutralized and dried; and (iii) the solid has been exposed to Soxhlet extraction with CH<sub>2</sub>Cl<sub>2</sub> (Merck, >99.8%) at 40 °C for 24 h. The extracts have been analyzed by GC  $\times$  GC in the apparatus described in section 2.1, following the protocol described in Table 2.

### 3. RESULTS AND DISCUSSION

**3.1. Effect of Deactivation.** Previous papers deal with the evolution of hydrocracking and hydrodesulfurization conversion with TOS for the catalysts used here.<sup>26,27</sup> For all of the catalysts, the conversion decreases within the initial 5 h TOS because of the catalyst deactivation. After this period, the catalysts reach a pseudo-stable state, in which they have a steady activity (during at least 24 h TOS). The remaining activity has a linear relationship with the remaining acidity of the catalysts.<sup>26</sup> The rate of deactivation and the remaining activity are dependent upon the reaction conditions, with the latter being higher when the temperature and H<sub>2</sub> pressure are increased.<sup>29</sup>

Figure 2 shows the component distribution in the feed (according to the carbon number) and the product distribution of LCO hydrocracking after 1 and 24 h TOS. The results correspond to the more pronounced deactivation profile for a run using the Y<sub>5</sub> catalyst, 400 °C, and 60 bar. After 1 h on stream, the catalyst displays a very high cracking rate; therefore, the products are short-chain hydrocarbons of ca. 4–5 carbon atoms. After 5 h on stream, the catalyst has a constant remaining activity, which allows the partial conversion of a heavy fraction of LCO (of more than 15 carbon atoms) into lighter products (of less than 13 carbon atoms), which is more appropriate for diesel blending. Despite the fact that the catalyst has a steady conversion after 5 h on stream, it is interesting to understand the mechanism of deactivation occurring within the initial 5 h, because it leads to a more rational understanding of the catalytic performance.

**3.2. Characterization of Deactivating Species.** The deactivating species deposited on the bifunctional catalyst in the hydrocracking of LCO have a very complex composition and nature. However, the term coke includes bulky hydrocarbons (usually called coke) and poisons as heteromolecules with nitrogen or sulfur. The characterization of this complex

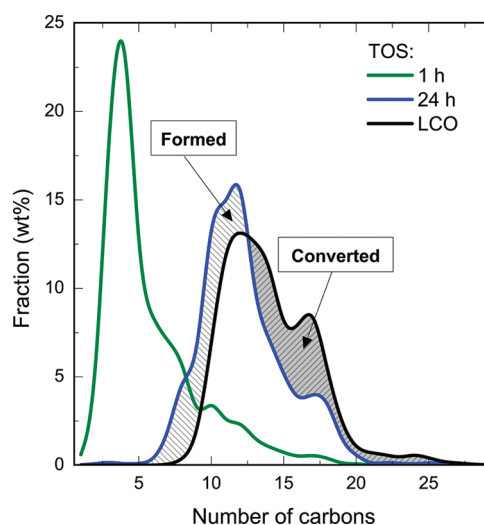


**Figure 2.** Carbon number distribution in the LCO and hydrocracking products for 1 and 24 h TOS. Reaction conditions: catalyst, Y<sub>5</sub>; 400 °C; 2 g of catalyst; WHSV, 2 h<sup>-1</sup>; pressure, 60 bar; and  $n_{H_2}$ , 10 mol<sub>H<sub>2</sub></sub>/mol<sub>LCO</sub>.

mixture has been carried out combining different methodologies.

**3.2.1. Temperature-Programmed Oxidation (TPO).** The TPO is widely employed for analyzing the condensation level of coke and its heterogeneity, in such a way that, the higher the combustion temperature, the lower the H/C ratio of the coke; i.e., the coke is more developed or has a higher condensation level. The peak width is associated with (i) the heterogeneity of coke composition and (ii) the apparent activation energy of the combustion. Besides, the temperature of the peaks in the TPO curves is influenced by diffusional limitations related to the coke structure (when coke is well-developed) and to the coke location in the porous structure of the catalysts. Thus, the combustion temperature is higher according to the following order of location in the catalyst: micropores > mesopores > macropores > outside of the zeolite crystals. These facts are well-known in the coke deposition on acid catalysts, especially for cracking catalysts (HY zeolites) and catalysts based on HZSM-5 zeolites used in the transformation of methanol,<sup>42,43</sup> bioethanol,<sup>44,45</sup> bio-oil,<sup>46</sup> and waste plastics.<sup>47,48</sup> into hydrocarbons and olefins. In all of these reactions on acid zeolites, the distribution of the catalyst acid strength has an influence on the development of coke.<sup>30,31</sup> In addition to the coke formation step in the cracking catalysts, the heavier polyaromatic compounds in the LCO, such as pyrenes (see Figure 1), behave as coke precursors, so that they are trapped or adsorbed on the catalyst.

In the literature related to the TPO of the coke deposited on bifunctional catalysts, the peak of low combustion temperature is associated with the coke deposited on the metallic function of the catalyst.<sup>49,50</sup> The peaks at higher temperatures are associated with different development levels of the coke in the micro-, meso-, and macropores in the acid function of the catalyst.<sup>51,52</sup>

Figure 3 shows the profiles of combustion of the Y<sub>5</sub> deactivated catalyst in terms of TG and MS (flow of exhaust gases) data. The pretreatment of the deactivated catalysts has been carried out at 550 °C with He, which is required for removing the significant content of adsorbed volatile compounds. It has been proven that these compounds

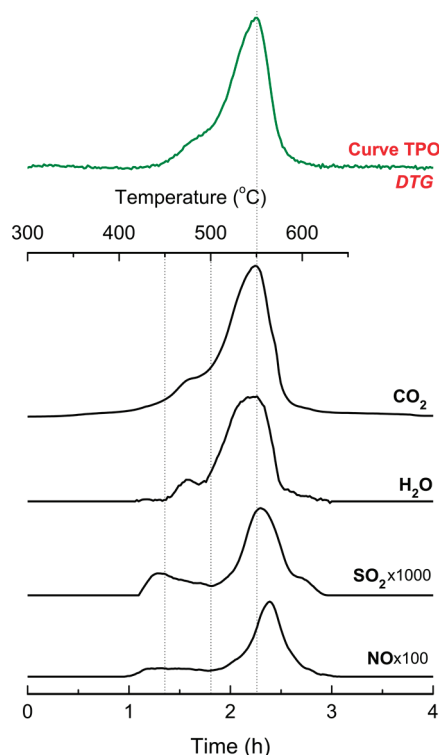
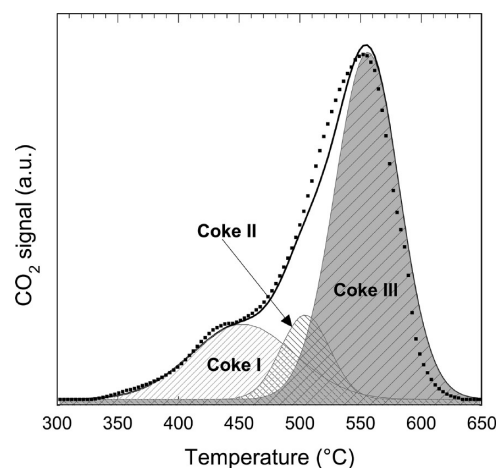


**Figure 3.** TPO curve and gaseous product flow for coke combustion. Reaction conditions: catalyst,  $Y_5$ ; 400 °C; WHSV, 2  $\text{h}^{-1}$ ; pressure, 60 bar;  $n_{\text{H}_2}$ , 8.9  $\text{mol}_{\text{H}_2}/\text{mol}_{\text{LCO}}$ ; and TOS, 24 h.

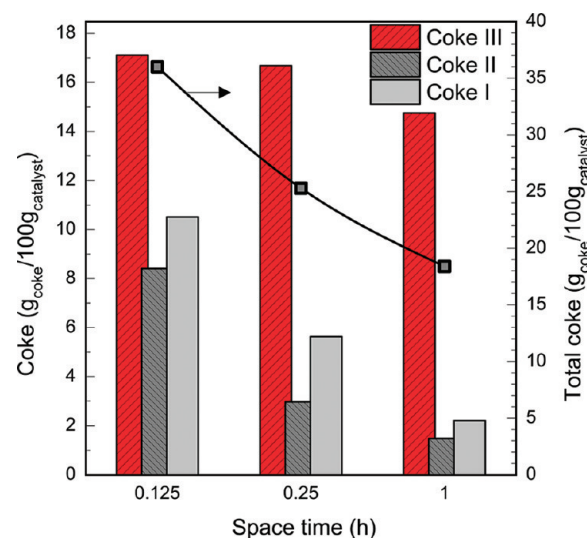
(which may account for 10–20 wt % of the fresh catalyst) do not contribute to catalyst deactivation because the catalyst does not recover the initial activity after their sweeping. The results in Figure 3 show complete combustion of the coke. The profiles of  $\text{SO}_2$  and  $\text{NO}$ , with peaks located at temperatures slightly higher than that of the main peak, the  $\text{CO}_2$  peak at 550 °C, reveal the presence of S and N in the polyaromatic compounds of heavy molecular weight in the coke, whose combustion requires high temperatures. On the contrary, the peak situated at 475 °C for  $\text{H}_2\text{O}$  formation is related to the combustion of aliphatic compounds in the coke.

Figure 4 shows the deconvolution results of the TPO curve shown in Figure 3. The deconvolution has been performed using Matlab, and three peaks are located at 450, 500, and 550 °C. According to the classification by Bauer and Karge,<sup>53</sup> each peak corresponds to a different type of coke (higher condensation level with the increase of the temperature): type I, at 450 °C; type II, at 500 °C; and type III, at 550 °C. According to the aforementioned criterion and considering the hypotheses established in the literature for other reaction systems with bifunctional catalysts,<sup>49,50</sup> coke I is related to the less developed coke (lowest aromatic condensation) and, therefore, its combustion occurs at lower temperatures. Coke III is related to the most developed coke.

On the basis of the high content of coke III in the  $Y_5$  catalyst (0.25  $\text{g}_{\text{coke}}/\text{g}_{\text{cat}}$ ; Figure 5) and the micropore volume of the same catalyst (0.25  $\text{cm}^3/\text{g}_{\text{cat}}$ ; Table 3), we have considered that a great fraction of coke III is a developed coke located outside of the zeolite particles. Furthermore, the high remaining activity of these catalysts in the pseudo-stable state supports this hypothesis, because external coke does not block either the metallic or the acid sites of the catalyst. Consequently, for the  $Y_5$  catalyst, the values of hydrocracking conversion of heavy-



**Figure 4.** Deconvolution of TPO results (same profile as in Figure 3) in three types of coke. Experimental conditions: catalyst,  $Y_5$ ; 350 °C,  $n_{\text{H}_2}$ , 8.9  $\text{mol}_{\text{H}_2}/\text{mol}_{\text{LCO}}$ ; pressure, 45 bar; and TOS, 24 h.



**Figure 5.** Effect of the space time on the distribution of coke fractions. Experimental conditions: catalyst,  $Y_5$ ; 350 °C,  $n_{\text{H}_2}$ , 8.9  $\text{mol}_{\text{H}_2}/\text{mol}_{\text{LCO}}$ ; pressure, 45 bar; and TOS, 24 h.

cycle oil (HCO) and hydrodesulfurization conversion are as high as 85 and 80%, respectively, in the pseudo-stable state.<sup>17</sup> The genesis of the external coke have two routes: deposition of the biggest molecules of the feed or carbocation chemistry on the acid sites. These molecules (coke precursors) migrate throughout the surface of the catalyst and, when placed outside of the zeolite, develop (without any steric hindrance) during bimolecular reactions, i.e., alkylation and hydrogen transfer.

Different factors may influence the fact that the combustion of the coke takes place at higher temperatures: (i) its condensed structure, with low H/C ratio, (ii) the diffusional limitations for oxygen into the zeolite micropores, partially occluded by coke, and (iii) the adsorption of the molecules of this coke on the acid sites. It is well-known that HY zeolites allow for the development of coke toward polyaromatic structures because of the hydrogen-transfer capacity of the acid sites and also the spatial capacity of the “cages” (with a diameter of 1.24 nm) that make up the intersections between the channels of the zeolite crystals.<sup>31,54</sup>

Figure 5 compares the contents of each type of coke obtained by integration for three different values of the space time. The remaining experimental conditions used are the same. As observed, the content of coke I decreases when the space time is increased, which supports the hypothesis that the coke I is mainly constituted by the bulky molecules in the LCO that are not able to diffuse within the pores of the HY zeolite and, therefore, are adsorbed on the external surface of the catalyst particles. When space time is increased, the hydrocracking of these molecules is enhanced, as well as that of coke precursors deposited on the metallic sites (coke type I or II, whose content also decreases). Likewise, the content of coke III also decreases when space time is increased, although to a lesser extent. This is due to the decrease in the coke precursor concentration along the catalytic bed, which, in turn, lowers the capacity to form coke (especially coke types I and II) at higher space time values. This dependency of the coke content with space time (or with the reaction media composition) is typical of the deactivation occurring in parallel to the main reaction; i.e., coke is preferably formed from reactants rather than the products.

**3.2.2. UV–Vis Spectroscopy.** The results of UV–vis spectroscopy corresponding to the deactivated catalysts (certain catalyst samples studied in Figures 4 and 5) are shown in Figure 6. The broad band at 200–300 nm is attributed to the catalyst

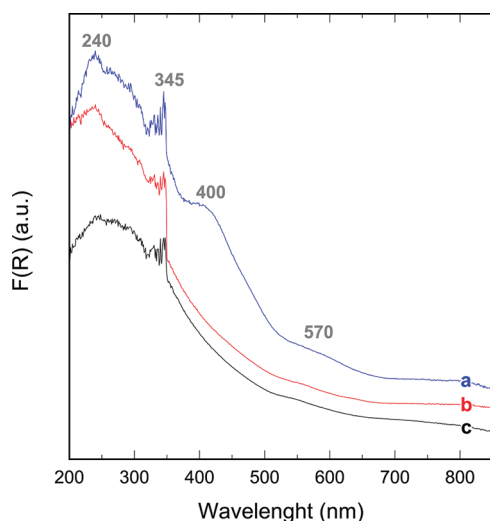


**Figure 6.** Effect of the space time on the UV–vis spectroscopic profiles: (a) space time, 0.125 h; (b) space time, 0.25 h; and (c) space time, 1 h. Experimental conditions: catalyst,  $Y_5$ ; 350 °C,  $n_{H_2}$ , 8.9 mol $_{H_2}$ /mol $_{LCO}$ ; pressure, 45 bar; TOS, 24 h; and WHSV, 2 h $^{-1}$ .

and to the double-conjugated bounds of the coke.<sup>53,55</sup> Mores et al.<sup>56</sup> have related the bands in the range of 345–500 nm to aromatic compounds: (i) the band at 345 nm corresponds to single-ring aromatics; (ii) the band at 400 nm corresponds to two- and three-ring aromatics; and (iii) the band at 500 nm corresponds to four-ring and higher aromatics. It is observed that, when space time is increased, the intensity of the bands corresponding to polyaromatic compounds of the coke (400 and 500 nm) decreases, which is consistent with the lower content of different types of coke when space time is increased (Figure 5). These polyaromatic structures of more than four rings have structural limitations for growing inside of HY zeolite; therefore, they are related to external coke.

**3.2.3. TPO–FTIR.** FTIR spectroscopy expands the information on the processes involved during the combustion of coke (TPO).<sup>49</sup> Figure 7 shows the vibrational spectra of the deactivated catalyst at different stages of the TPO, corresponding to the deactivated  $Y_5$  catalyst, using a record frequency of 12 h $^{-1}$ , with a resolution of 4 cm $^{-1}$ . Figure 7a displays the range of the spectrum of 1300–1700 cm $^{-1}$ , and Figure 7b displays the range of the spectrum of 2700–3400 cm $^{-1}$ . For the FTIR spectrum at 100 °C (start of the experiment) the following bands are identified: 1382 cm $^{-1}$ , C–H bonds of branched aliphatic groups (symmetric); 1450 cm $^{-1}$ , C–H bonds of –CH $_2$  groups (asymmetric); 1598 cm $^{-1}$ , C–C bonds of polycondensed aromatics; 2854 cm $^{-1}$ , C–H bonds of –CH $_2$  groups (symmetric); 2925 cm $^{-1}$ , C–H bonds of –CH and CH $_2$  groups (asymmetric); 2960 cm $^{-1}$ , C–H bonds of CH $_3$  (asymmetric); 3050 cm $^{-1}$ , C–H bonds of aromatics; 3160 cm $^{-1}$ , C–H bonds close to heteroatoms of S or N (symmetric); and 3245–3315 cm $^{-1}$ , N–H bonds of heteroatomic molecules (symmetric).

The bands for wavenumbers below 3000 cm $^{-1}$  decrease throughout the temperature ramp. At the same time, the FTIR bands corresponding to hydroxyl groups of the zeolite become more intense (results not shown here) because of catalyst regeneration. Besides, the evolution of the composition of the coke remaining throughout combustion is noteworthy. Thus, there are two different circumstances extensively studied in the literature regarding the combustion of coke deposited on the acid catalysts, which are also observed here: (i) the preferential combustion of coke with a lower H/C ratio<sup>50,57</sup> and (ii) the aging of the compounds of the remaining coke when they are under a gas flow at a high temperature, by means of pyrolysis and hydrogen transfer, with a decrease in the H/C ratio.<sup>58,59</sup> The preferential combustion of aliphatic compounds is observed for temperatures above 100 °C, with a remarkable decrease in the intensity of the bands corresponding to the aliphatic compounds of the coke, which disappear at 450 °C. The band of branched aliphatics at 1450 cm $^{-1}$  overlaps with the bands of other chemical bonds, making any qualitative analysis impossible. Most of the C–H bonds disappear in the range of 250–400 °C. The bands of N-containing groups indicate that they burn off in parallel to the aliphatic groups. However, the bands of the polycondensed aromatics (1580 cm $^{-1}$ ) of the coke do not change noticeably until 250 °C.

The intensity of the bands at 3050 and 3160 cm $^{-1}$ , corresponding to single-ring aromatics and heteroatoms, decrease in the range of 100–250 °C. At higher temperatures, they increase to levels higher than those of the original coke. The band at 3050 cm $^{-1}$  peaks at 400 °C, and the band at 3160 cm $^{-1}$  peaks at 425 °C.

**3.2.4. Composition of the Soluble Coke.** Figure 8 shows the chromatogram of the coke fraction soluble in dichloromethane (after destruction of the inorganic structure of the catalyst with HF), which has been extracted from the deactivated  $Y_5$  catalyst. This fraction corresponds to 30 wt % of the total amount of coke. There is a significant amount of four-ring aromatics, with pyrenes and benzofluorenes being the most abundant compounds. The content of aromatics of more than five rings, such as methyl-benzo[*j*]aceanthrylene, 3-methyl-benzo[*g,h,i*]perylene, and 4-methyl-indene[1,2,3-*c,d*]fluoranthene, is also noteworthy. The most relevant hydrocarbons in the soluble fraction of the coke are summarized in Table 4. Table 5 shows the heteroatomic compounds of the soluble coke. The fraction of molecules with nitrogen or sulfur is considerably



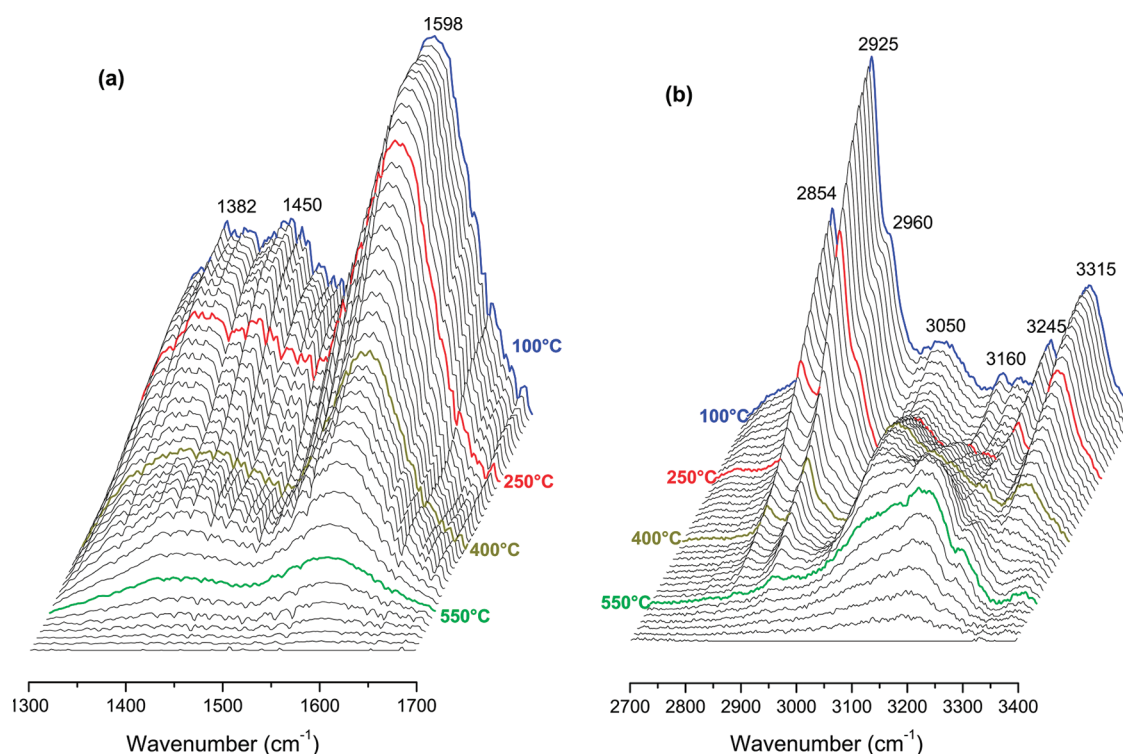


**Figure 7.** FTIR analysis evolution in the coke combustion: (a) 1300–1700  $\text{cm}^{-1}$  and (b) 2700–3400  $\text{cm}^{-1}$ . Experimental conditions: catalyst,  $Y_S$ ; 350  $^{\circ}\text{C}$ ;  $n_{\text{H}_2}$ , 8.9  $\text{mol}_{\text{H}_2}/\text{mol}_{\text{LCO}}$ ; pressure, 45 bar; TOS, 24 h; and WHSV, 2  $\text{h}^{-1}$ .

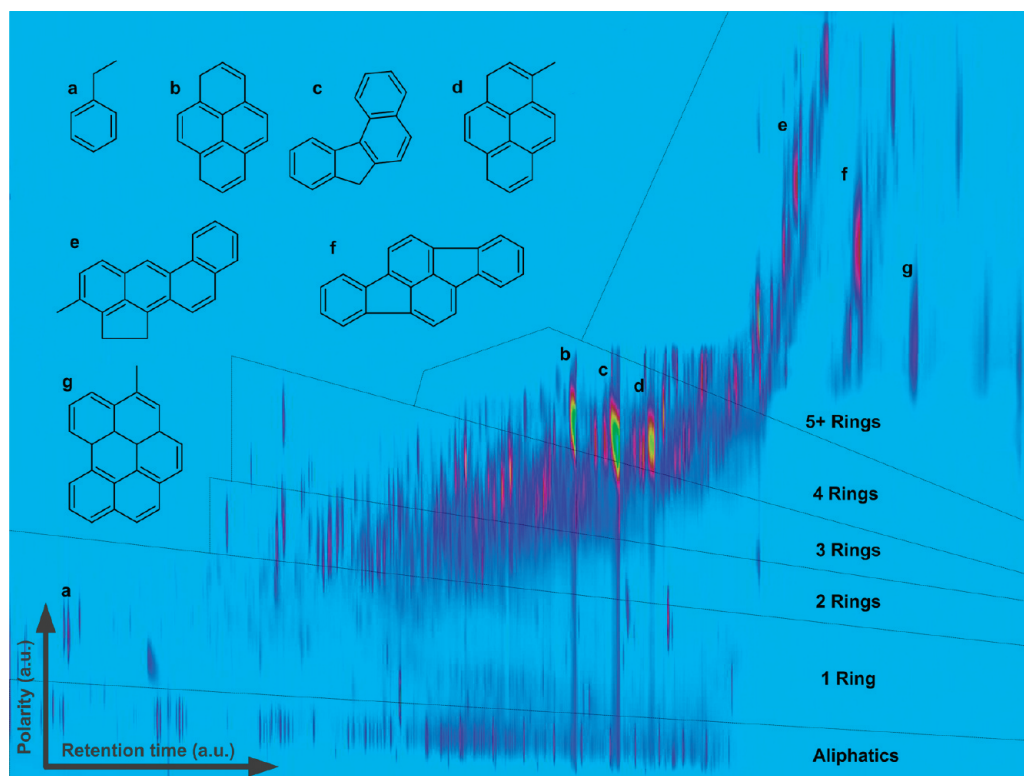


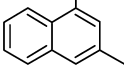
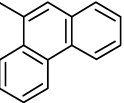
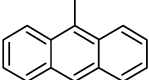
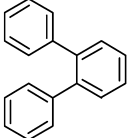
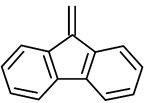
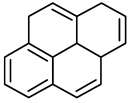
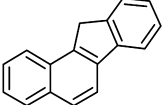
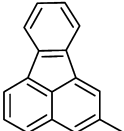
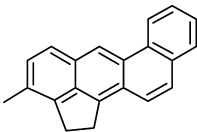
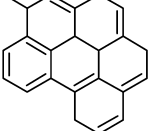
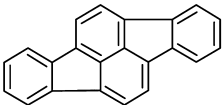
**Figure 8.** GC  $\times$  GC/MS analysis results of the coke soluble in dichloromethane. Reaction conditions: catalyst,  $Y_S$ ; 350  $^{\circ}\text{C}$ ,  $n_{\text{H}_2}$ , 8.9  $\text{mol}_{\text{H}_2}/\text{mol}_{\text{LCO}}$ ; pressure, 45 bar; TOS, 24 h; and WHSV, 2  $\text{h}^{-1}$ .

lower than that of hydrocarbons. Among these compounds, the most abundant families correspond to amines, quinolones, indoles, and thiazoles.

The comparison between soluble coke composition (Figure 8) to that of the LCO (Figure 1) reveals a higher molecular weight and condensation level of the compounds in this coke fraction, which correspond mainly to the coke deposited on the



Table 4. Main Hydrocarbon Compounds in the Soluble Coke Extracted from the Deactivated Catalyst Using Dichloromethane

Name	Structure	Formula	g mol <sup>-1</sup>	# CAS
1,3 dimethyl-naphtalene		C <sub>12</sub> H <sub>12</sub>	156	575-41-7
9 methyl-fenantrene		C <sub>15</sub> H <sub>12</sub>	192	883-20-5
9 methyl-antracene		C <sub>15</sub> H <sub>12</sub>	192	779-02-2
o-terphenyl		C <sub>18</sub> H <sub>14</sub>	230	84-15-1
9 methylene 9H-fluorene		C <sub>14</sub> H <sub>10</sub>	178	4425-82-5
pyrene		C <sub>16</sub> H <sub>10</sub>	202	129-00-0
11H-benzo[a]fluorene		C <sub>17</sub> H <sub>12</sub>	216	238-84-6
2-methyl-fluoranthene		C <sub>17</sub> H <sub>12</sub>	216	33543-31-6
3 methyl-benzo[j]aceanthrylene		C <sub>21</sub> H <sub>14</sub>	266	3343-10-0
4 methyl-benzo[g,h,i]perylene		C <sub>23</sub> H <sub>14</sub>	290	19224-38-5
indene[1,2,3-cd]fluoranthene		C <sub>22</sub> H <sub>12</sub>	276	193-43-1

external surface of the catalyst particles and is a result of a significant condensation of the LCO compounds catalyzed by the acid sites of the HY zeolite located outside of the catalyst particles.

### 3.2. Effect of Catalyst Properties on Coke Formation.

Using the hydroprocessing conditions described before, the conversion of LCO is 81% for Y<sub>5</sub>, 56% for Y<sub>12</sub>, 49% for B, 32% for A, and 20% for the F catalyst. This conversion correlates linearly with the acidity of the catalyst.<sup>26</sup> At the same time, all of the catalysts show an increase of the cetane number up to 34–38 and a significant yield of high-quality gasoline with an octane number higher than 92.<sup>26</sup> The difference in coke yields is a

function of the activity of the catalyst, as well as the concentration of precursors in the reaction medium. Even in the scenario of having the same conversion of LCO, the selectivity is a function of the support<sup>27</sup> and the concentration of species in the reactor is, thus, different for each catalyst. Each species has an intrinsic rate of coke formation; therefore, it is not straightforward to compare the yields of coke at the same activity and selectivity of the catalyst in this kind of complex reactions.

The aforementioned results reveal the significance of the concentration of different coke precursors in the reactor (a consequence of catalyst activity) on coke deposition and its

Table 5. Main Heteroatomic Compounds in the Soluble Coke Extracted from the Deactivated Catalyst

Name	Structure	Formula	g mol <sup>-1</sup>	# CAS
2-[2,4-dimethyl-phenyl]indole		C <sub>16</sub> H <sub>15</sub> N	221	62663-29-0
p,p'-ditolylamine		C <sub>18</sub> H <sub>14</sub>	230	64401-21-4
5,8-dimethyl-quinoline		C <sub>11</sub> H <sub>11</sub> N	157	2623-50-9
4-phenyl-2-[4-tolylamino]-thiazole		C <sub>16</sub> H <sub>14</sub> N <sub>2</sub> S	266	16098-04-7
1-[phenylthio]-naphthalene,		C <sub>16</sub> H <sub>12</sub> S	236	7570-98-1

composition. Figure 9 shows the TPO profiles (as CO<sub>2</sub> evolution profiles) for the catalysts deactivated under the

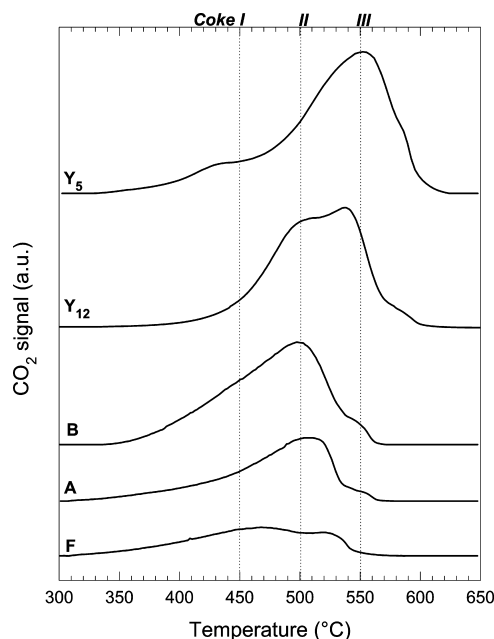


**Figure 9.** TPO curves for different catalysts. Reaction conditions: 400 °C; WHSV, 2 h<sup>-1</sup>; pressure, 60 bar; and  $n_{H_2}$ , 10 mol<sub>H<sub>2</sub></sub>/mol<sub>LCO</sub>.

same conditions as in the previous results. As for the Y<sub>5</sub> catalyst (Figure 4), three types of coke are observed in the TPO curve of the deactivated catalysts, i.e., cokes I, II, and III, corresponding to combustion temperatures of 450, 500, and 550 °C, respectively. The exception is the F catalyst (a commercial FCC catalyst as the support), which does not have the peak at 550 °C (coke type III).

Figure 10 shows the areas integrated for each type of coke in the curves in Figure 9. The results in Figure 10 show that the support has a considerable effect on the composition of the coke. The deactivated F catalyst has 2.5 wt % of coke, which is a

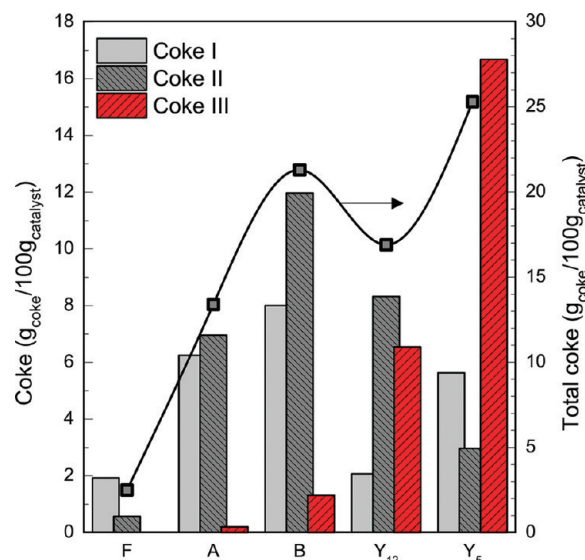


**Figure 10.** Effect of the catalyst support in the fractions of deposited coke. Reaction conditions: 350 °C,  $n_{H_2}$ , 8.9 mol<sub>H<sub>2</sub></sub>/mol<sub>LCO</sub>; 45 bar; TOS, 24 h; and WHSV, 2 h<sup>-1</sup>.

much lower amount than that for the remaining catalysts, and does not have coke type III. This result is a consequence of the lower acidity of the catalyst (Table 3), where coke is originated. Furthermore, this catalyst has a low concentration of acid sites, particularly of strong acid sites (Table 3). The deactivated A catalyst has a greater amount of coke, 13.41 wt %, which is related to the higher amount of coke type I (5.94 wt %) and type II (6.25 wt %). This fact is consistent with the higher value of total acidity, which seems to have a significant role in the deposition of these coke types. However, this catalyst has a very low concentration of strong acidity (Table 3), responsible for forming coke type III inside the pores of the alumina. The higher total acidity and strong acidity of the B catalyst also explains the higher deposition of coke types I and II. Besides, the H $\beta$  zeolite used as a support in the B catalyst has a remarkable level of strong acidity, which provides a significant

hydrocracking activity to the catalyst. These strong acid sites are active in the condensation reactions of coke precursors toward polyaromatic structures (coke type III). The  $Y_{12}$  catalyst has a high content of coke type III, whose formation is attributed to the high acid strength and hydrogen-transfer capacity of the HY zeolite. These are decisive for activating the condensation of coke precursors toward polyaromatic structures. The significance of the acid strength is a deciding factor, and the  $Y_5$  catalyst has a higher content of coke III than the  $Y_{12}$  catalyst, which is due to the higher acidity of  $Y_5$  than  $Y_{12}$  (Table 3). The formation of coke III, mainly located outside the zeolite crystals as mentioned above, is enhanced by the strong acid sites of the catalyst, which explains the higher content of coke type III in the catalysts based on the HY zeolite. Strong acid sites participate in the formation of coke precursors, which migrate throughout the surface of the catalyst and develop further outside of the zeolite.

In this discussion, we have indicated that the properties of the acidic function (support) is the key for understanding the deactivation in this process. Our previous results using the same catalysts<sup>26</sup> allow us to state that the reactions on the acidic sites are controlling the final activity of the catalyst; indeed, the amount of coke deposited on the catalyst is linearly dependent upon the acidity of the catalyst.<sup>26</sup> The metallic function also plays a role in deactivation, because it hydrogenates the aromatics and olefins, which are promoters of coke.<sup>34</sup> Bimetallic catalysts based on Pt–Pd are more active, stable, and selective than the monometallic counterparts.<sup>26</sup> However, among the catalysts studied here, the differences in the properties of the metallic function are not sufficient to discriminate the effect of the metal on the deactivation. The higher activity in the pseudo-stable regime of the bimetallic Pt–Pd catalyst is due to the interaction of the two metals, which make the catalyst more resistant toward sulfur poisoning. The ratio of Pt–Pd is a crucial parameter in this respect, and as such, our future work will investigate the effect of the metallic properties on the hydroprocessing of LCO.

#### 4. CONCLUSION

The coke deposited on Pt–Pd/zeolite bifunctional catalysts in the hydrocracking of an aromatic-rich feed (LCO) has a very complex composition made up of polyaromatic hydrocarbons with heteroatoms (sulfur and nitrogen). However, according to the profiles of coke combustion (TPO), a simplification in three types has been made, which are related to peaks in the combustion rate at 450, 500, and 550 °C. The three types of coke observed by TPO correspond to different condensation levels and locations within the catalytic surface (on the external surface, on the metallic sites, and inside the micropores of the catalyst), although these types of cokes cannot be related exclusively to their location. The composition, nature, and location of these cokes have been characterized using TG–TPO combined with MS and FTIR spectroscopy.

The analysis of soluble coke (in dichloromethane) reveals the presence of more condensed products than those of LCO, mainly pyrene. The condensation of coke takes place on both the outside and inside of the porous structure of the support.

The properties of the catalysts affecting coke composition are mainly pore topology of the support and acidity. The acid sites (concentration and strength) of the catalyst favor simultaneously: (i) the condensation of coke precursors in the micropores of the catalysts, (ii) the growth of internal and external coke, and (iii) the hydrocracking of coke. As a result,

after 5 h on stream, the catalysts show a steady conversion of LCO in terms of hydrocracking and hydrotreating.

The Pt–Pd/HY catalyst with a low  $SiO_2/Al_2O_3$  ratio and, therefore, high values of total acidity and acid strength provides the highest values of steady hydroconversion of LCO. The explanation is that this catalyst has the highest activity for hydrocracking both the feed and the coke.

The information obtained is of special interest for striking a balance between the hydrocracking of LCO and coke precursors. Furthermore, this study on the nature and evolution of coke on bifunctional catalysts means a step further into the knowledge of the optimization of catalyst composition.

#### AUTHOR INFORMATION

##### Corresponding Author

\*Telephone: +3494601-8435. E-mail: pedro.castano@ehu.es.

##### Notes

The authors declare no competing financial interest.

#### ACKNOWLEDGMENTS

The authors acknowledge the late Prof. F. M. Ramôa Ribeiro for his inspiring work. The research was carried out with the financial support of the Ministry of Science and Education of the Spanish Government (Projects CTQ2006-03008/PPQ and CTQ2010-19623), the University of the Basque Country (UFI 11/39) and the Basque Government (Project GIC07/24-IT-220-07).

#### REFERENCES

- (1) Speight, J. *The Refinery of the Future*, 1st ed.; Elsevier, Inc.: Amsterdam, The Netherlands, 2011; Chapters 9 and 10.
- (2) Gruia, A. In *Handbook of Petroleum Processing*; Jones, D. S. J., Pujadó, P. R., Eds.; Springer: Dordrecht, The Netherlands, 2006; Chapter 7.
- (3) Mederos, F. S.; Rodríguez, N. A.; Ancheyta, J.; Arce, E. *Energy Fuels* **2006**, *20*, 936–945.
- (4) Šimáček, P.; Kubička, D. *Fuel* **2010**, *89*, 1508–1513.
- (5) Šimáček, P.; Kubička, D.; Kubičková, I.; Homola, F.; Pospíšil, M. *Fuel* **2011**, *90*, 2473–2479.
- (6) Calemme, V.; Gambaro, C.; Parker, W. O. Jr.; Carbone, R. *Catal. Today* **2010**, *149*, 40–46.
- (7) Castaño, P.; Pawelec, B.; Fierro, J. L. G.; Arandes, J. M.; Bilbao, J. *Appl. Catal., A* **2006**, *315*, 101–113.
- (8) Castaño, P.; Gutiérrez, A.; Pawelec, B.; Fierro, J. L. G.; Aguayo, A. T.; Arandes, J. M. *Appl. Catal., A* **2007**, *333*, 161–171.
- (9) Castaño, P.; Zepeda, T. A.; Pawelec, B.; Makkee, M.; Fierro, J. L. G. *J. Catal.* **2009**, *267*, 30–39.
- (10) Jin, H.; Yi, X.; Sun, X.; Qiu, B.; Fang, W.; Weng, W.; Wan, H. *Fuel* **2010**, *89*, 1953–1960.
- (11) Li, B.; Li, X.; Xu, J.; Pang, X.; Gao, X.; Zhou, Z. *J. Colloid Interface Sci.* **2010**, *346*, 199–207.
- (12) Zhang, X.; Guo, Q.; Qin, B.; Zhang, Z.; Ling, F.; Sun, W.; Li, R. *Catal. Today* **2010**, *149*, 212–217.
- (13) Barrón, A. E.; Melo-Banda, J. A.; Domínguez, J. M.; Hernández, E.; Silva, R.; Reyes, A. I.; Meraz, M. A. *Catal. Today* **2011**, *166*, 102–110.
- (14) Tiwari, R.; Rana, B. S.; Kumar, R.; Verma, D.; Kumar, R.; Joshi, R. K.; Garg, M. O.; Sinha, A. K. *Catal. Commun.* **2011**, *12*, 559–562.
- (15) Elizalde, I.; Rodríguez, M. A.; Ancheyta, J. *Appl. Catal., A* **2010**, *382*, 205–212.
- (16) Elizalde, I.; Ancheyta, J. *Fuel* **2011**, *90*, 3542–3550.
- (17) Zhao, Y.; Wei, F.; Zhang, S.; Yu, Y. *Fuel* **2011**, *90*, 1900–1906.
- (18) Jiménez-García, G.; Aguilar-López, R.; Maya-Yescas, R. *Fuel* **2011**, *90*, 3531–3541.
- (19) Muzíková, Z.; Procházka, F.; Pospíšil, M. *Fuel* **2010**, *89*, 3534–3539.

- (20) Albertazzi, S.; Baraldini, I.; Busca, G.; Finocchio, E.; Lenarda, M.; Storaro, L.; Talon, A.; Vaccari, A. *Appl. Clay Sci.* **2005**, *29*, 224–234.
- (21) Laredo, G. C.; Saint-Martin, R.; Martinez, M. C.; Castillo, J.; Cano, J. L. *Fuel* **2004**, *83*, 1381–1389.
- (22) Fujikawa, T.; Idei, K.; Ohki, K.; Mizuguchi, H.; Usui, K. *Appl. Catal., A* **2001**, *205*, 71–77.
- (23) Nylén, U.; Sassu, L.; Melis, S.; Järas, S.; Boutonnet, M. *Appl. Catal., A* **2006**, *299*, 1–13.
- (24) Nylén, U.; Pawelec, B.; Boutonnet, M.; Fierro, J. L. G. *Appl. Catal., A* **2006**, *299*, 14–29.
- (25) Calemma, V.; Giardino, R.; Ferrari, M. *Fuel Process. Technol.* **2010**, *91*, 770–776.
- (26) Gutiérrez, A.; Arandes, J. M.; Castaño, P.; Aguayo, A. T.; Bilbao, J. *Energy Fuels* **2011**, *25*, 3389–3399.
- (27) Gutiérrez, A.; Arandes, J. M.; Castaño, P.; Olazar, M.; Bilbao, J. *Fuel* **2011**, DOI: 10.1016/j.fuel.2011.10.010.
- (28) Gutiérrez, A.; Arandes, J. M.; Castaño, P.; Olazar, M.; Barona, A.; Bilbao, J. *Fuel Process. Technol.* **2012**, *95*, 8–15.
- (29) Gutiérrez, A.; Arandes, J. M.; Castaño, P.; Olazar, M.; Barona, A.; Bilbao, J. *Chem. Eng. Technol.* **2011**, DOI: 10.1002/ceat.201100382.
- (30) Guisnet, M.; Magnoux, P. *Appl. Catal., A* **2001**, *212*, 83–96.
- (31) Guisnet, M.; Costa, L.; Ramôa Ribeiro, F. J. *Mol. Catal. Chem.* **2009**, *305*, 69–83.
- (32) Peeters, E.; Cattenot, M.; Geantet, C.; Breysse, M.; Zotin, J. L. *Catal. Today* **2008**, *133*, 299–304.
- (33) Castaño, P.; Pawelec, B.; Fierro, J. L. G.; Arandes, J. M.; Bilbao, J. *Fuel* **2007**, *86*, 2262–2274.
- (34) Aguayo, A. T.; Castaño, P.; Mier, D.; Gayubo, A. G.; Olazar, M.; Bilbao, J. *Ind. Eng. Chem. Res.* **2011**, *50*, 9980–9988.
- (35) Castaño, P.; Elordi, G.; Ibañez, M.; Olazar, M.; Bilbao, J. *Catal. Sci. Technol.* **2012**, DOI: 10.1039/C2CY00434H.
- (36) Valle, B.; Gayubo, A. G.; Alonso, A.; Aguayo, A. T.; Bilbao, J. *Appl. Catal., B* **2010**, *100*, 318–327.
- (37) Emeis, C. A. J. *Catal.* **1993**, *141*, 347–354.
- (38) Castaño, P.; Arandes, J. M.; Pawelec, B.; Fierro, J. L. G.; Gutiérrez, A.; Bilbao, J. *Ind. Eng. Chem. Res.* **2007**, *46*, 7417–7425.
- (39) Gutiérrez, A.; Castaño, P.; Azkoiti, M. J.; Bilbao, J.; Arandes, J. M. *Chem. Eng. J.* **2011**, *176–177*, 302–311.
- (40) Guisnet, M.; Costa, L.; Ribeiro, F. R. J. *Mol. Catal. A: Chem.* **2009**, *305*, 69–83.
- (41) Holmes, S. M.; Garforth, A.; Maunders, B.; Dwyer, J. *Appl. Catal., A* **1997**, *151*, 355–372.
- (42) Benito, P. L.; Gayubo, A. G.; Aguayo, A. T.; Olazar, M.; Bilbao, J. *Ind. Eng. Chem. Res.* **1996**, *35*, 3991–3996.
- (43) Valle, B.; Castaño, P.; Olazar, M.; Bilbao, J.; Gayubo, A. G. J. *Catal.* **2011**, *285*, 304–314.
- (44) Gayubo, A. G.; Alonso, A.; Valle, B.; Aguayo, A. T.; Olazar, M.; Bilbao, J. *Fuel* **2010**, *89*, 3365–3372.
- (45) Gayubo, A. G.; Alonso, A.; Valle, B.; Aguayo, A. T.; Bilbao, J. *Appl. Catal., B* **2010**, *97*, 299–306.
- (46) Gayubo, A. G.; Valle, B.; Aguayo, A. T.; Olazar, M.; Bilbao, J. *Energy Fuels* **2010**, *23*, 4129–4136.
- (47) Elordi, G.; Olazar, M.; Lopez, G.; Castaño, P.; Bilbao, J. *Appl. Catal., B* **2011**, *102*, 224–231.
- (48) Castaño, P.; Elordi, G.; Olazar, M.; Aguayo, A. T.; Bilbao, J. *Appl. Catal., B* **2011**, *104*, 91–100.
- (49) Martin, N.; Viniegra, M.; Lima, E.; Espinosa, G. *Ind. Eng. Chem. Res.* **2004**, *43*, 1206–1210.
- (50) Martin, N.; Viniegra, M.; Zarate, R.; Espinosa, G.; Batina, N. *Catal. Today* **2005**, *107–108*, 719–725.
- (51) Ereña, J.; Sierra, I.; Olazar, M.; Gayubo, A. G.; Aguayo, A. T. *Ind. Eng. Chem. Res.* **2008**, *47*, 2238–2247.
- (52) Sierra, I.; Ereña, J.; Aguayo, A. T.; Olazar, M.; Bilbao, J. *Appl. Catal., B* **2010**, *94*, 108–116.
- (53) Bauer, F.; Karge, H. G. *Mol. Sieves* **2007**, *5*, 249–363.
- (54) Cerqueira, H. S.; Caeiro, G.; Costa, L.; Ramôa Ribeiro, F. J. *Mol. Catal. A: Chem.* **2008**, *292*, 1–13.
- (55) Palumbo, L.; Bonino, F.; Beato, P.; Bjørgen, M.; Zecchina, A.; Bordiga, S. *J. Phys. Chem. C* **2008**, *112*, 9710–9716.
- (56) Mores, D.; Kornatowski, J.; Olsbye, U.; Weckhuysen, B. M. *Chem.—Eur. J.* **2011**, *17*, 2874–2884.
- (57) Ortega, J. M.; Gayubo, A. G.; Aguayo, A. T.; Benito, P. L.; Bilbao, J. *Ind. Eng. Chem. Res.* **1997**, *36*, 60–66.
- (58) Magnoux, P.; Cerqueira, H. S.; Guisnet, M. *Appl. Catal., A* **2002**, *235*, 93–99.
- (59) Aguayo, A. T.; Gayubo, A. G.; Ereña, J.; Atutxa, A.; Bilbao, J. *Ind. Eng. Chem. Res.* **2003**, *42*, 3914–3921.